International Journal of Heat and Mass Transfer 221 (2024) 125095

Contents lists available at ScienceDirect

International Journal of Heat and Mass Transfer

journal homepage: www.elsevier.com/locate/ijhmt

Preparation and assessment of ionic liquid and few-layered graphene composites to enhance heat and mass transfer in adsorption cooling and desalination systems

Handsome Banda [a,b], Tahmid Hasan Rupam [c,d], Ahmed Rezk [a,b,*], Zoran Visak [e], James Hammerton [e], Qingchun Yuan [a,e], Bidyut Baran Saha [f,g]

[a] Energy and Bio-products Research Institute (EBRI), College of Engineering and Physical Science, Aston University, Birmingham B4 7ET, UK
[b] Mechanical, Biomedical and Design Engineering Department (MBDE), College of Engineering and Physical Science, Aston University, Birmingham B4 7ET, UK
[c] Department of Mechanical and Aerospace Engineering at the University of Missouri, Columbia, MO 65211, USA
[d] Multiphysics Energy Research Center (MERC), University of Missouri, Columbia, MO 65211, USA
[e] College of Engineering and Physical Science, Aston Advanced material research institute, Aston University, Birmingham B4 7ET, UK
[f] International Institute for Carbon-neutral Energy Research (WP1-12CNER), Kyushu University, 744 Motooka, Nishi-ku, Fukuoka 819-0395, Japan
[g] Mechanical Engineering department, Kyushu University, 744 Motooka, Nishi-ku, Fukuoka 819-0395, Japan

ARTICLE INFO

Keywords:
Adsorption refrigeration
Composite sorbents
Graphene
Ionic liquids
Water

ABSTRACT

Adsorption systems can utilise low-temperature renewable and waste heat sources, which have emerged as a feasible alternative to conventional water desalination and cooling systems. However, the material of poor heat and mass transfer performance stall their widespread utilisation. This article presents the development and investigation of new composites employing few-layered graphene platelets and ionic liquids, namely ethyl-methylimidazolium methane sulfonate ([EMIM][CH3SO3]) and Ethyl-methylimidazolium-chloride ([EMIM][Cl]) to address such challenges. The impact of the few-layered graphene platelets, thermal properties, water adsorption properties of the developed composites and their thermal diffusivity were experimentally investigated. Besides, the overall cyclic performance was studied experimentally at the material level and computationally at the component level by employing a previously validated 2D dynamic heat and mass transfer model. The experimental investigation indicated that pristine few-layered graphene has a surface area of 56.8978 m^2/g and a relatively high thermal diffusivity of 22.23 mm^2/s. The developed composites showed higher thermal diffusivity than the baseline adsorbent silica gel. The highest thermal diffusivity was 11.84 mm^2/s for GP-CH_3SO_3-10, 394 times higher than silica gel. Water adsorption characteristics of the composites were carried out, and the Dubinin–Astakhov (D-A) model was employed to model the experimental isotherms with good accuracy. The cumulative advanced adsorption and thermal characteristics of the developed composites resulted in higher cyclic performance by up to 82 % and 85 % than that of the baseline silica gel.

1. Introduction

Adsorption desalination and cooling systems have emerged as the most feasible alternative to conventional reverse osmosis, multi-stage flash and multi-effect desalination for water and vapour compression systems for cooling [1]. The main reason for the perceived success of the adsorption desalination and cooling is its ability to utilise solar energy and low-grade waste heat below 100 °C, minimum use of electricity and use of environmentally friendly working fluids [1–3]. However, although adsorption systems have the advantages mentioned above, they are characterised by low thermal efficiency emanating from poor heat and mass transfer, resulting in low process efficiency [4–6]. The performance of adsorption systems is strongly linked to the sorption pair's behaviour: adsorption isotherms and kinetics [7]. Considerable research has been undertaken to improve the component-level adsorption cooling and water desalination systems [8]. Researchers have also focussed on investigating different types of packed bed designs, including plate heat exchangers (HE), honeycomb HE, fin-tube HE and coated HE [9]. However, some researchers have proposed applying the

* Corresponding author at: Mechanical, Biomedical and Design Engineering Department (MBDE), College of Engineering and Physical Science, Aston University, Birmingham B4 7ET, UK
E-mail address: a.rezk@aston.ac.uk (A. Rezk).

https://doi.org/10.1016/j.ijheatmasstransfer.2023.125095
Received 7 August 2023; Received in revised form 21 September 2023; Accepted 13 December 2023
Available online 23 December 2023

Nomenclature

C_p	specific heat capacity [kJ $kg^{-1}K^{-1}$]
d_i	tube diameter [mm]
d_o	tube diameter [mm]
D_s	surface diffusivity [m^2 s^{-1}]
D_{so}	pre-exponential coefficient [m^2 s^{-1}]
E_a	activation energy [kJ mol^{-1}]
h	enthalpy [kJ kg^{-1}]
h_f	height [mm]
l	tube length [mm]
K	thermal conductivity [W m^{-1} K^{-1}]
K_o	adsorption constant [KPa^{-1}]
$k_s\alpha_\nu$	diffusion time constant
M	mass [kg]
$\dot{m}$	mass flowrate [kg/s]
P	pressure [Pa]
p	fin pitch [mm]
Q	heat transmitted [J]
Q_{st}	heat of adsorption [kJ kg^{-1}]
R	gas law constant [kJ $kmol^{-1}K^{-1}$]
t	time [s]
T	temperature [K] [°C]
q	uptake [kg kg^{-1}]
q_o	equilibrium uptake [kg kg^{-1}]
R_p	particle radius [m]

Greek

μ	dynamic viscosity [Pa s]
ρ	density [kg m-3]
α	thermal diffusivity [mm^2 s -1]
δ	fin thickness [mm]
ν_g	specific volume [m^3 kg^{-1}]

Subscripts

ad	adsorbent
ads	adsorption
cw	cooling water
chw	chilled water
cond	condenser
des	desorption
evap	evaporator
f	fin

GP/IL graphene nanoplatelete /ionic liquid

hex	heat exchanger
hw	heating water
i	inner
in	inlet
o	outer
out	outlet
sat	saturation
SG	silica gel

concept of a fluidised bed to enhance the heat and mass transfer in an adsorbent bed [10,11]. Fluidisation involves the creation of a suspension of solid particles in the fluid stream, i.e. liquid or gas, within a fluidised bed to increase their chemical and physical interaction. Kryzwanski et al. [12] investigated the heat and mass transfer in fluidised beds for cooling and desalination employing artificial intelligence (AI) simulation to envisage the processes inside the adsorption bed, which showed significant enhancement of the adsorption desalination and cooling by improving the convective heat transfer to 1212.62 Wm^{-1} K and high water uptake of up to 1.65 g/g.

However, the level of performance achieved in adsorption desalination and cooling systems is still insufficient to warrant its commercialisation. Many researchers have studied different adsorbents to enhance the performance of adsorption desalination and cooling systems, for instance, silica gel and metal organic frameworks [3,8,13,14].

Intensive work has been carried out to enhance the performance of adsorbents by making composites by impregnating the host matrixes like Zeolite, Silica gel and activated carbon with hygroscopic salts such as $CaCl_2$, $MgCl_2$, $MgSO_4$, $LiNO_3$, LiCl and LiBr [15–17]. For instance, Aristov et al. [18] studied silica gel impregnated with $LiNO_3$ as a new adsorbent composite $LiNO_3$/silica KSK (SWS-9L) for cooling and reported a 6 % increase in cooling capacity compared to SG/water pair. Tanashev et al. [15] investigated Silica gel KSK impregnated with three salts: $CaCl_2$, $MgCl_2$ and LiBr. The three composites increased thermal conductivity 3–4 times compared to silica gel, and water adsorption increased from 0.05 to 0.7–0.9 kg/kg. Chan et al. [16] investigated a Zeolite 13X and $CaCl_2$ composite for adsorption cooling systems. Their findings showed a 34 % increase in SCP compared to pure Zeolite 13X and an 81 % increase in COP. Tso et al. [17] investigated composites for adsorption cooling by impregnating AC and Silica with $CaCl_2$ at different concentrations. Their results showed an enhancement of SCP by 372 % and COP by 92 %. Apart from composite from conventional adsorbents, researchers have developed composite utilising carbon nanotubes (CNT) [19]. CNTs are lightweight cylindrical molecules composed of hexagonal hybridized carbon atoms which can be formed by either rolling a single sheet or multi sheets of graphene [20]. CNT has unique properties, including high thermal conductivity ranging from 1500 to 6000 W/mK, thermal stability, efficient heat transfer resistance, a well-developed pore structure and attractive functional water transport capability [21,22].

Of late, there has been ample research on enhancing the thermal properties of adsorbents by developing new composites using various additives [23]. Graphene has attracted considerable interest as it can be modified through reactions with different functional groups to form various derivatives [24–26]. Graphene and its graphene platelets derivative (GP) showed substantial heat transfer properties, reaching 3000 Wm^{-1} K^{-1} making them attractive for many applications, including adsorption systems [27]. Generally, graphene is a two-dimensional monoatomic sheet of carbon atoms arranged in a honeycomb structure with electrons in sp^2 hybridised orbit. These electrons have the lowest energy level, implying high stability, high strength and high intrinsic mobility of 15,000 cm^{-2} at room temperature, enhancing thermal transport properties [27]. Graphite, for instance, is an allotrope consisting of large number of graphene layers and can be used as a feedstock for graphene synthesis [27,28]. Graphene is economically demanding to produce, which has given rise to commercially viable derivatives, such as GP, being considered as its alternative in some applications [29,30] .

GPs have a planar shape and are made from a few layers of graphite with a thickness from 0.1 to 100 nm [31]. El-sharkawy et al. [32] investigated the performance of a composite made from 20 % Expanded graphite, 50 % Maxsorb III (a highly porous activated powder)and 10 % Polyvinyl alcohol. They found that the composite improved thermal conductivity by 11 times more than pure Maxsorb III [32]. Pal et al. [23] developed an activated carbon composite using graphene nanoplatelets and polyvinyl alcohol (PVA) to experimentally investigate the impact of GP on the composite's thermal conductivity, porous properties and adsorption uptake. Their findings showed that the composite had an enhanced thermal conductivity of 23.5 times and an ethanol volumetric uptake 23 % higher than pure activated carbon (AC) [23,33].

Ionic liquids (IL) are molten salts comprising inorganic/organic anions and cations. IL are known to have unique properties such as low

vapour pressure, high thermal stability (due to their ionic structure) and high viscosity [34,35]. The thermal stability, as well as the high sorption potential (water solvation) of hydrophilic ILs, have motivated the investigation for hydrophilic ILs use as absorbents with water refrigerant [34,36], but also in developing sorption composites for desalination and cooling systems. Thus, Askalany et al. [37] investigated the water uptake of composite made from IL [EMIM][CH3SO3] and Syloid AL-1FP silica at different concentrations of IL from 1.8 wt% to 60 wt%. It was reported that the specific daily water production (SDWP) increased by 1.7 times than pure silica gel. Askalany et al. [38] experimentally investigated the adsorption properties of silica-supported ionic liquid called EMIM-AC/Syloid 72 FP. A high SDWP of 47 m^3 day^{-1} ton^{-1}, a coefficient of performance (COP) of 0.85 and a specific cooling power (SCP) of 600 Wkg^{-1} were reported. Pal et al. [39] investigated polymerised ionic liquid as a binder on consolidated activated carbon composites with improved packing density. Their investigation showed an 85 % enhancement in thermal conductivity and a higher volumetric uptake of 22 % than pure activated carbon.

While the above literature has shown that using GP and IL, individually, in composites can improve the thermal or sorption properties, there is no reported achievement in developing composites of advanced adsorption simultaneously with thermal characteristics, which hardly any research has proposed. Therefore, the higher thermal diffusivity of GP and IL's thermal stability, solvation and low vapour pressure has motivated this work to develop composites comprising GP and IL and cover the identified research gap.

The present study aims to develop a novel sorption composite comprised of GP host matrix and hydrophilic ILs 1-Ethyl-3-methylimidazolium methanesulfonate [EMIM][CH_3SO_3] or 1-Ethyl-3-methylimidazolium chloride [EMIM][Cl], as sorbents. The rationale is that the GP enhances thermal diffusivity while ILs significantly increase the sorbate loading. The main aim of this research and its novelty is to develop an understanding of utilising GP/IL composites for sorption cooling and desalination and their impact on enhancing the heat and mass transfer properties of the sorption/desorption processes. Therefore, the objectives of the study are to (1) experimentally investigate the thermal characteristics and physical properties of GP to be used as a host matrix; (2) develop GP/IL composites and investigate their sorption and thermal characteristics, benchmarking them against Silica gel as baseline sorbent; (3) study the impact of varying the IL content on the overall sorption and thermal performance of the composites; (4) determine the material and component levels overall cyclic performance experimentally and by using 2D computational heat and mass transfer modelling.

2. Materials and methodology

This work investigates a composite that comprises few-layered graphene (GP) and Ionic liquids (IL). The ILs, 1-Ethyl-3-methylimidazolium methane sulfonate ([EMIM][CH_3SO_3]) and 1-Ethyl-3-methylimidazolium-chloride ([EMIM][Cl]) were purchased from Acros organics and Sigma Aldrich, respectively. A host material for the IL was a few-layered pristine graphene platelets of 1–5 2D layers, commercially known graphene nanoplatelets obtained from Graphitene Ltd. The pristine GP was selected for use as a host structure based on its experimentally determined superior thermal diffusivity of 22.3 mm^2/s and high BET surface area of 56.8978 m^2/g, compared to other graphene derivatives and Silica gel as shown in Fig. 2 and Table 1. The composites were benchmarked against Fuji Silica gel (SG) of a widely used adsorbent of 0.18–1 mm particle size.

Table 1
Physical properties of pristine few-layered graphene platelets (GP and Graphite).

Nanoparticle	BET area (m^2/g)	Thermal diffusivity (mm^2/s)	Thermal conductivity (W/mK)
GP	56.8978	22.23	7.36
Graphite	22.5668	4.92	4.57

Silica gel (SG) has been widely used as an adsorbent due to its low cost, reliability and high uptake compared with conventional adsorbents. It is the most popular for commercial applications in adsorption chillers, adsorption desalination, drying and separation [19,40,41]. SG is a polymeric porous material with a colloidal silicic acid structure and has SiOH and SiOSi functional groups, allowing it to absorb water and alcohol adsorbates. One of the attributes of SG is the ability to adsorb water 35–40 % of its dry mass and has an adsorption capacity regarded as highly stable under long operation periods. Its regenerative capability at a low temperature of 50–90 °C makes it suitable for adsorption applications utilising low heat sources. Given the broad utilisation of silica gel, it was considered the baseline adsorbent for benchmarking the developed adsorbents, which facilitates prorating the developed composites' performance against other adsorbents such as zeolite and metal-organic frameworks (MOFs).

A simple two-bed sorption cooling and water desalination configuration was considered to determine the cyclic performance, as shown in Fig. 1. The two-bed system continuously supplies cooling and clean water, as one bed operates at each cycle.

2.1. Composite synthesis

The wet impregnation method was employed to develop the sorption composites due to its ability to attain a high level of Interfacial/bulk deposition onto the host matrix. Firstly, 1 g of the host matrix was dried at 150 °C for 12 h. Ionic liquid's aqueous solutions were developed at a concentration of 10 wt% to 30 wt%. To enable the wet impregnation process, the total volume of the aqueous solution was 25 mm^3, which sufficiently exceeded the volume of the dried matrix. Secondly, the dried host matrix was immersed into the aqueous solution and steered for 1 h to attain a homogenous host matrix/aqueous solution mixture. Thirdly, the developed mixture was left to rest for an hour to ensure the complete impregnation of the host matrix. Finally, the excess solution was filtered, and the composite was dried gently at 150 °C for 1 h. Table 2 shows the range of the developed composites based on different ionic liquid concentrations using a host matrix of few-layered graphene platelets.

3. Composites properties experimental analysis

3.1. SEM imaging

Scanning electronic microscope (SEM) enabled visualising and understanding the influence of the ionic liquid intercalation into the host

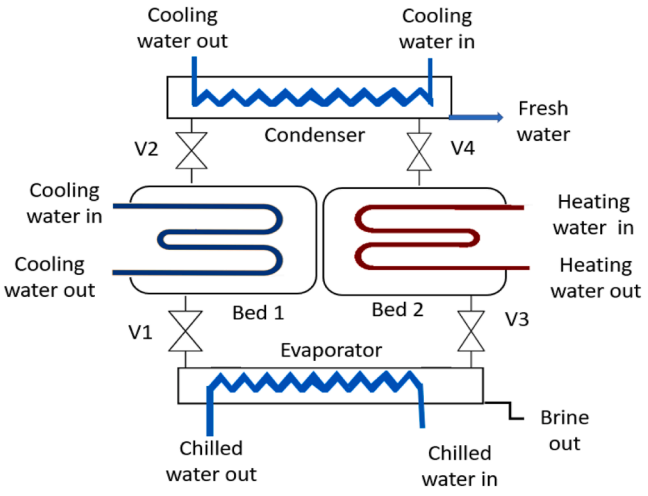

Fig. 1. Schematic diagram of the adsortption cooling and water desalination system.

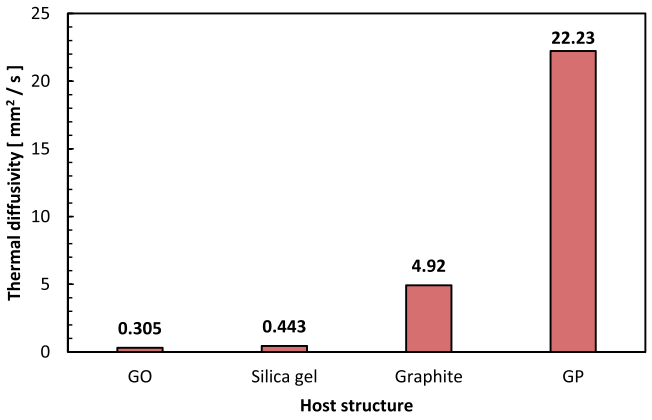

Fig. 2. Comparison of thermal diffusivity of the host matrixes.

Table 2
The range of composite developed.

GP + [EMIM][Cl] composite		GP + [EMIM][CH_3SO_3] composite	
Composite name	[EMIM][Cl] concentration	Composite name	[EMIM][CH_3SO_3] concentration
GP-CL-10	10 %	GP- CH_3SO_3-10	10 %
GP-CL-20	20 %	GP- CH_3SO_3-20	20 %
GP-CL-30	30 %	GP- CH_3SO_3-30	30 %

matrix. Fig. 3 shows the SEM images for the developed composites impregnated with different concentrations of IL. Fig. 3a– indicate an uneven surface and cavities for the composites with an ionic liquid concentration of 30 % and less for both [EMIM][Cl] and [EMIM][CH_3SO_3]. The cavities indicate that the composites are highly heterogeneous and have a high possibility of the IL being confined into the host matrixes' interlayer spaces; hence, no over-impregnation occurred. However, ionic liquid concentration above 30 % led to accumulating ILs on the surface of the host material, as shown in for 40 % IL concentration. The host matrix is smooth and fully covered with the ionic liquid, indicating the host matrix's over-impregnation.

3.2. XRD crystallographic analysis

The prepared composites were subjected to powder XRD analysis to examine the crystal structure of the GP in the composites, as shown in Fig. 4. The diffraction of every sample shows the structure characteristic of graphite indicated by the diffraction peak 002 at $2\theta = 26.4–26.6^{o}$, and 100 and 101 peaks at $2\theta = 42.3–42.4^{o}$ and $44.4–44.6^{o}$, respectively. The peaks of the pristine GP are slightly smaller than that of its composites with the ILs; the latter increases with the content of ILs towards that of perfect graphite. The characteristic diffraction angle increases imply that the impregnation of the ILs does not change the layered crystal structure of the GP but plays a role in driving the GP structure towards perfection. Furthermore, the GP-CL-30 composites show a series of diffraction peaks at $2\theta = 5.39$, 10.72, 14.19 16.36 and 21.42 ^{o},which may indicate that some [EMIM][CL] molecules have intercalated into the graphene layers at the surface of GP.

3.3. Ionic liquid contents

Thermogravimetric analysis (TGA) was employed to determine each composite's final ionic liquid content. Analysis was performed using a TGA 8000^{TM} (PerkinElmer) with a nitrogen furnace purge of 40 mL/min to prevent oxidation or combustion reactions of the sample during the heating program. A heating rate of 20 °C/min was used across the range of interest for the composites (200–400 °C for [EMIM][Cl], 200–550 °C for [EMIM][CH_3SO_3]). Inorganic residues in the composites were investigated by switching the furnace purge gas to oxygen above 650 °C and continuing heating to a final temperature of 950 °C.

The ionic liquid content of the developed composites was determined by Eq. (1), and the results are shown in Fig. 5. It can be seen in Fig. 5 that the greater the weight percentage of ionic liquid in the aqueous solution during graphene impregnation, the higher the ionic liquid content of the composites. The increase of final ionic liquid content in the composites is not linear with the increasing fraction of ionic liquid in the aqueous impregnation solution, suggesting that the host matrix approaches saturation, aligning with observations in the SEM experimentation. No inorganic residues were observed in any of the composites or raw materials.

$$IL\ content = \frac{mass_{IL}}{mass_{GP}} \times 100 \quad (1)$$

3.4. Composites heat transfer properties

The thermophysical properties, including the thermal diffusivity, were experimentally investigated to determine the dynamic thermal response potential of the developed composite. The thermal diffusivity was determined using NETZSCH LFA 467 Hyper Flash Laser flash analyser (LFA). The LFA 467 comprises a laser source, furnace, infrared detector, data control and acquisition unit. Fig. 6 shows a simplified schematic diagram and a pictorial view of the LFA. The Laser flash method uses a transient heat flux technique to measure the thermal diffusivity. A high-intensity laser pulse strikes the sample's front face, and the adsorbed heat travels through the sample thickness, resulting in a temperature increase at the rear face. The increase in temperature on the rear face is detected by an infrared detector and recorded in the data acquisition unit. The thermal diffusivity of the composites was measured at a temperature range of 25–100 °C. The experiment was performed three times with five laser shots at each temperature for the repeatability check. The repeated measurements show close values with 0.01 standard deviation, where the mean value for the three tests was used to represent the thermal diffusivity. Table 3 shows the experimentally determined thermal diffusivity of the composites compared to the SG benchmark. There was a significant increase in thermal diffusivity in all the composites compared to SG due to the presence of, primarily, GP. It can also be observed that the 10 %wt composite had the highest thermal diffusivity, followed by the 20 % wt, and the 30 % wt composites showed the least. The 10 %wt composite had the highest thermal diffusivity because it had the lowest IL content; therefore, the impact of the relatively lower thermal diffusivity of IL, concerning GP, was experienced less in the 10 % than the other composites with higher IL concentrations. It agrees with the findings on the thermal diffusivity of IL by Zhao et al. [42], which reported IL of lower thermal diffusivity than GP but higher than metal salts. It highlights the benefit of investigating ILs as a replacement for the conventionally used metal salts to support the sorption simultaneously with the heat transfer characteristics.

The thermal diffusivity test temperature range of 25–100 °C showed the impact of temperature on the thermal diffusivity of the composites. The composites of up to 65 %wt IL content (i.e., GP-Cl-30 and GP-CH_3SO_3-30) remained stable under high temperatures of up to 100 °C, even though the thermal diffusivity decreases slightly with increasing temperature, unlike SG, which remains constant at that temperature range. On the other hand, composites of IL content above 65 %wt experienced a separation of the impregnated ionic liquids at the higher temperature, which supports the earlier discussion about composites' over-impregnation when utilising high IL concentration (i.e., GP-Cl-40 and GP-CH_3SO_3-40). It also could be worsened by the thermal expansion of the IL at temperatures above 55 °C at high IL concentrations above the 30 % threshold. Therefore, the temperature range for thermal diffusivity measurement for GP-Cl-30 and GP-CH_3SO_3-30 narrowed to

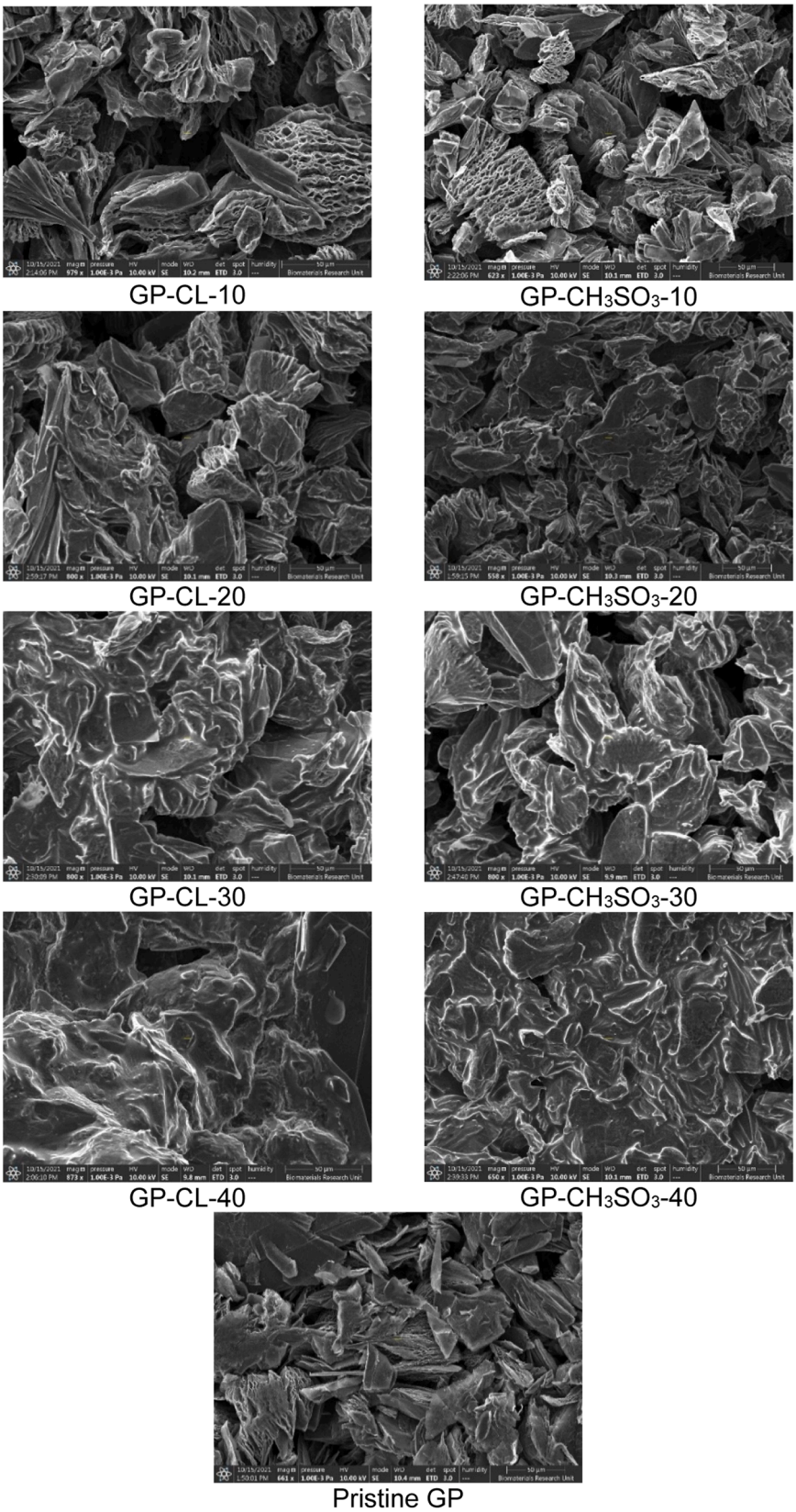

Fig. 3. . SEM image of pristine graphene and few-layered graphene nano platelets/ Ionic liquid composites.

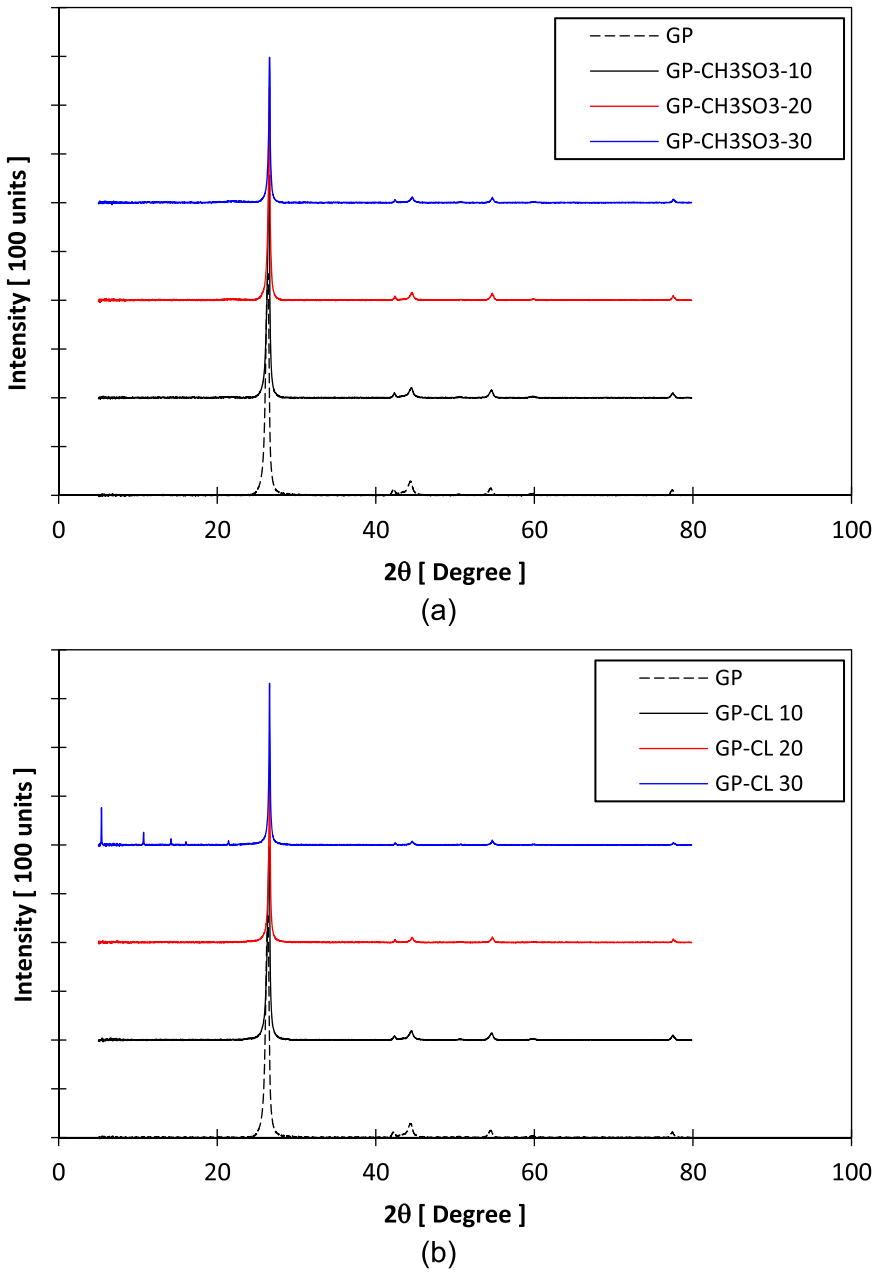

Fig. 4. XRD results of the developed composites of (a) GP-CH_3SO_3 and (b) GP-CL.

25–55 °C. However, it should not be misconstrued as limiting the adsorbent's usability at higher temperatures up to 30 %wt range. Remarkably, during regeneration at 85 °C, which exceeds the 55 °C threshold, the IL within the composite retains its water capture capacity intact, while the composite cools down to 30 °C for the subsequent adsorption cycle, the IL contracts and returns to its original state within the host graphene nanoplatelet (GNP) matrix, highlighting the reversible and robustness of the adsorption process. Therefore, the composite investigation was limited to up to GP-Cl-30 and GP-CH_3SO_3-30, which remained feasible. Fig. 7 shows the influence of temperature on the composites' thermal diffusivity.

3.5. Composites adsorption properties

The adsorption characteristics of the composites were determined using a gravimetric Dynamic Vapour Sorption analyser (DVS) shown in Fig. 8. The DVS equipment comprised a microbalance that measures the adsorbent mass to determine the instantaneous water vapour uptake/offtake during the adsorption/desorption processes. At the same time, the pressure ratio between the adsorbent and water vapour equivalent to P_{evap}/P_{bed} varied between 0.0 % and 90 % in steps of 10 %. Before the test, the DVS analyser microbalance accuracy was verified at ±0.05 mg using a 100 mg standard calibration mass. Dry Nitrogen purges the reaction and microbalance chambers before each test. The water uptake corresponding to vapour pressure values make up the adsorption isotherms and are generated by measuring the adsorbent mass at the condition of no change in adsorbent mass at a given water vapour pressure ratio. The sorption/desorption temperature remained constant at each isotherm. The vapour generation and the sample chamber are operated at thermal equilibrium within a single temperature enclosure to prevent condensation during the whole operation. The adsorption isotherm characteristics have been performed at 15 and 45 °C. Fig. 9 shows the experimentally measured equilibrium adsorption uptake for the GP-CL-10-30 and GP- CH_3SO_3-10-30 composites.

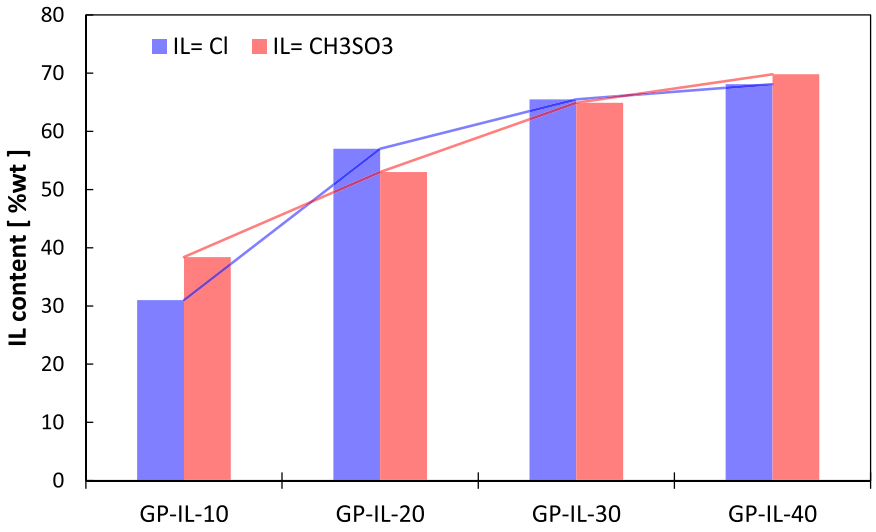

Fig. 5. ILs content in the developed composites.

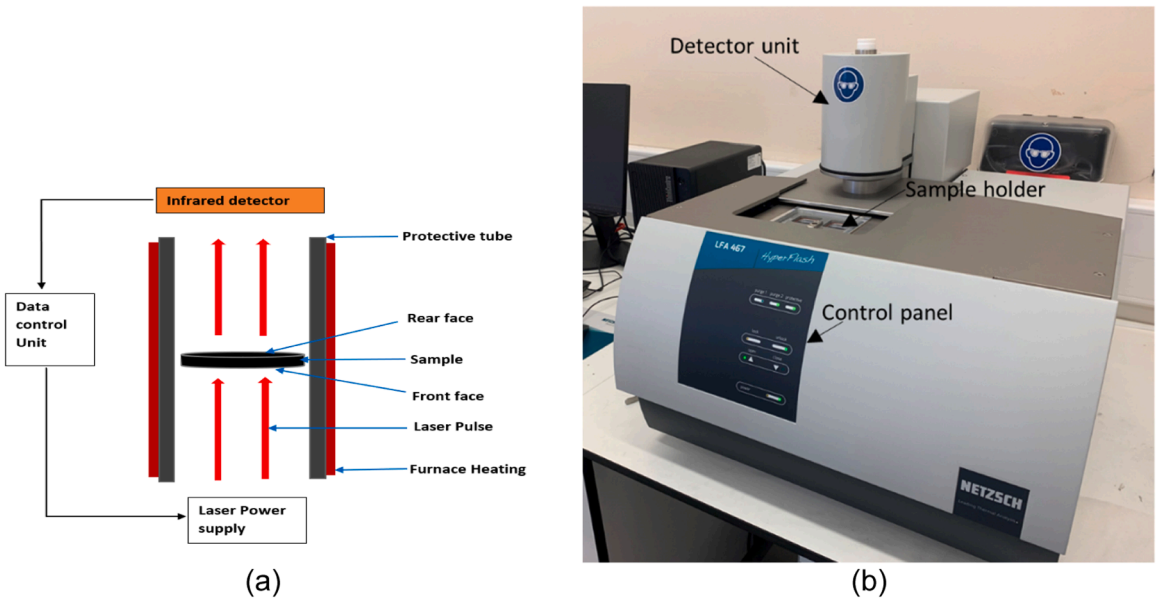

Fig. 6. . LFA 467 Laser Flash Analyser: (a) schematic diagram and (b) pictorial view.

Table 3
The thermal diffusivity values of the developed composites.

Material	Thermal diffusivity (mm^2/s)	Temperature range (°C)	Material	Thermal diffusivity (mm^2/s)	Temperature range (°C)
Silica gel (exp)	0.365	Room temp	Silica gel [43]	0.312	Room temp
GP-CL-10	9.96	25–100	GP-CH_3SO_3-10	11.84	25–100
GP-CL-20	6.78	25–100	GP-CH_3SO_3-20	6.40	25–100
GP-CL-30	5.98	25–55	GP-CH_3SO_3-30	5.92	25–55

The composites' gravimetric adsorption and desorption cycles were performed for 120 h, equivalent to 20 cycles. The pressure ratio P_{evap}/P_{bed} alternated between 0 % and 90 % extremes to determine the composite stability. All the composites showed a slightly low uptake in the first cycle and maintained a stable uptake percentage until the last cycle. The percentage difference between the highest and lowest uptake was less than 1 %, which shows that the developed composites are highly stable. Fig. 10 shows the gravimetric stability tests for the composites with IL content below 65 % (i.e., GP-Cl-30 and GP-CH_3SO_3-30) during adsorption and desorption.

3.5.1. Isotherm modelling

Isotherm modelling is essential to undertake further component and system-level analysis. Three predictive modelling approaches can be used to simulate the adsorption process: empirical modelling approach, molecular modelling approach, and machine learning approach (ML) using artificial intelligence (AI) [44]. The empirical modelling is used to fit adsorption isotherms to develop empirical correlations [45]. Molecular modelling considers the molecular interactions and the adsorption energies [46]. ML approach can be considered a black box learning model that utilises relatively large data for predicting the sorption

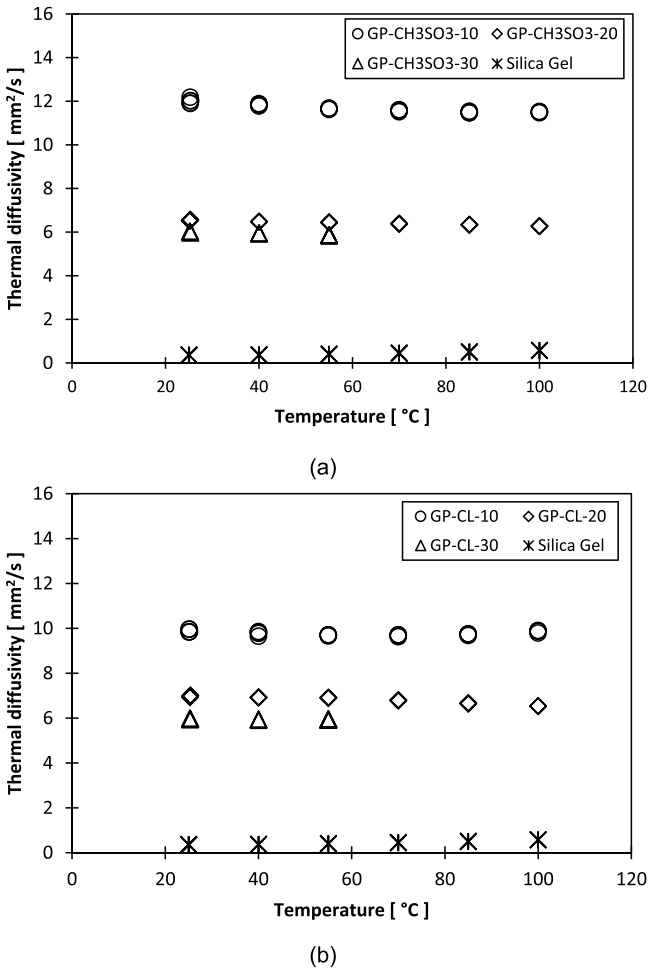

Fig. 7. Temperature dependant thermal diffusivity of the developed composites: (a) GP/[EMIM][CH_3SO_3], and (b) GP/[EMIM][Cl] composites compared with SG.

performance, such as the adsorption capacity and the solution equilibrium concentration [44]. AI models are highly accurate in simulating adsorption isotherms but are challenging in training, testing and validation tools, making it complicated [47]. They are usually valid within the specified training domain and inaccurate for over or under-predicting the sorption characteristics. This study used empirical modelling to simulate the adsorption isotherms, which is more straightforward and reliable to implement. Additionally, the primary purpose of this study was to evaluate the system performance of an adsorption chiller working with the novel composite adsorbents developed here.

Many empirical isotherm models have been developed to determine the isotherms based on several properties such as the heat of adsorption, temperature-dependent saturation, amount of loading to create a monolayer coverage per unit volume of the packing media (solid saturation loading) and adsorption equilibrium constant [7,48,49]. Examples of such models include Sips, Dubinin–Astakhov, Tóth, Henry, Freundlich, Langmuir, Temkin and Hill-de Boer; each broadly suits a specific isotherm type. In this study, the developed composites showed type II isotherm with water, which can be modelled using the Dubinin–Astakhov (D-A) adsorption isotherms model, as stated by Eq. (2) [50]. The D-A model originates from the Polanyi theory of multilayer adsorption potential for micropore filling [51]. D-A model was preferred in fitting the experimentally measured adsorption isotherm because of its ability to linearize adsorption data at varied pressure ranges while accurately relating the equilibrium pressure and adsorbed amount by the composites over the entire range of the micropore filling. Considering the heterogeneity of the developed composites and the restriction on the calculated maximum adsorption by the micropore filling in the composite, it was possible to obtain information about the micropore structure owing to the n exponent parameter of the D-A to fully describe the isotherms. Furthermore it is one of the most utilised isotherm model for modelling type II adsorption isotherms data [52]. On the other hand, in this study, the C-S-K adsorption isotherm model modified with the D-A isotherm model has been invoked to express the adsorption enthalpies of the studied pair as a function of adsorption uptake [53].

$$q = q_o \exp\left[-\left\{ \frac{RT}{E} \ln\left(\frac{P}{P_s}\right)\right\}^n \right] \quad (2)$$

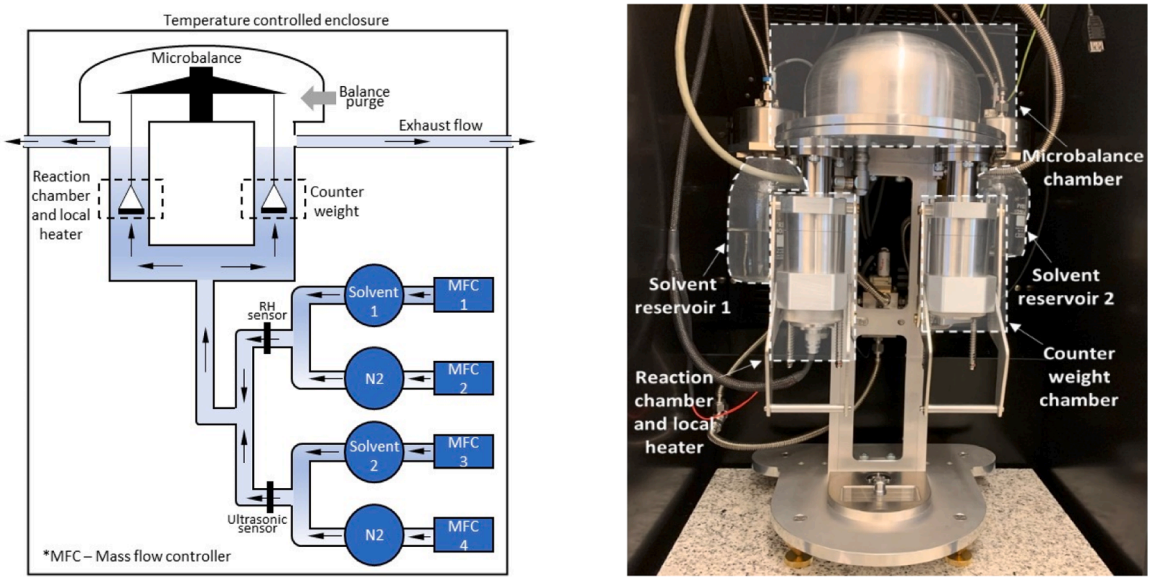

Fig. 8. . Dynamic vapor sorption analyser (a) Schematic diagram and (b) Pictorial view.

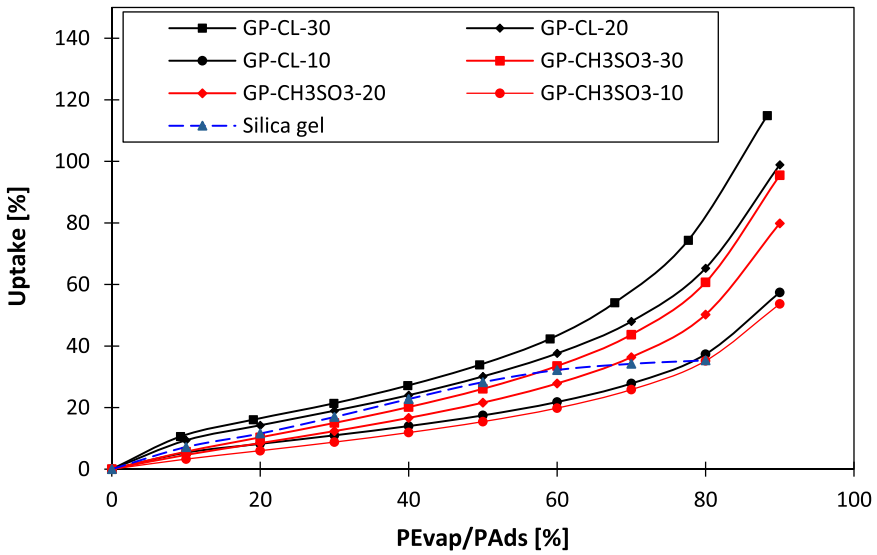

Fig. 9. . The adsorption isotherms for the developed composite and Fuji silica gel benchmark.

where, q (kg/kg) denotes adsorption uptake at a given temperature and corresponding pressure ratio; q_o is the equilibrium uptake (kg/kg); E is the characteristic energy of adsorption (KJmol^{-1}); P_s (kPa) is the saturation pressure at corresponding temperature and the index n is the structural heterogeneity coefficient.

In modelling the experimental isotherm data, a nonlinear optimisation method was employed for optimising the D-A model parameters for all the developed composite/water pairs. Table 5 shows the parameters of the D-A model employed in isotherm experimental data modelling with a regression parameter (R^2) of 0.9998. The developed isotherm model agrees well with the experimental adsorption isotherm of 0.05 mean deviation, as shown in Fig. 11.

The results show that GP-CL-30 has the highest equilibrium water uptake while CH_3SO_3-10 showed the least. The higher equilibrium water uptake in the GP-CL-30 is attributed to the high IL content in the composite. More IL content in the host matrix led to higher uptake, which agrees with the findings by Askalany et al. [37] in their study of silica gel/IL composites for desalination. The high uptake in the GP-CL-30 compared to all the GP-CH_3SO_3 shows that the CL-based IL interacts highly with water (i.e., solvation), resulting in higher water uptake. It was also observed that all the studied composites have significantly higher equilibrium uptake than baseline adsorbent silica gel, with the highest GP-CL-30 showing a 78 % enhancement. This can be attributed to the adsorption characteristics of IL, which allows more water sorption (Table 4).

3.5.2. Adsorption kinetics

The adsorption kinetics determine the rate of adsorption and desorption. The linear driving force (LDF) model, as shown in Eqn (3-5), is widely used and was acceptable for governing the adsorption kinetics for GP/IL composites and SG [6]

$$\frac{\partial \omega}{\partial t} = k_s \alpha_v \ (w^* - w) \tag{3}$$

$$k_s \alpha_v = 15 \frac{D_s}{R_p^2} \tag{4}$$

$$D_s = D_{so} exp\left(-\frac{E_a}{RT}\right) \tag{5}$$

Arrhenius's equation, Eq. (5), can be rearranged as shown in Eq. (6).

$$\ln D_s = \ln D_{so} - \frac{E_a}{RT} \tag{6}$$

where, $k_s \alpha_v$ is the diffusion time constant: The equilibrium uptake w^* (kg/kg) is determined from the D-A and modified Freundlich models for GP/IL and SG, respectively: w is the uptake at any given time; D_{so}(m^2 s^{-1}) is the pre-exponential coefficient; E_a (kJ/kg) is the activation energy; R (kJ.kmol^{-1}K^{-1}) is the universal gas constant; D_s (m^2 s^{-1}) is the surface diffusivity; R_p is the particle radius (m); T (K) is the adsorbent temperature. The constant 15 was used, as reported by Zhang et al. [54]. Since the adsorbent particles are spherical. As reported by El-Sharkawy et al. [55], the values of D_{so} and E_a were determined by the Arrhenius plot in which lnD_s is plotted against (1/T). The slope of the plot gives $\frac{E_a}{R}$ and the intercept gives the constant D_{so} based on Eq. (4). The LDF model's coefficients are given in Table 5.

3.5.3. Isosteric heat of sorption

Isosteric heat of sorption is defined as the heat released at a constant adsorbate amount. It is a critical thermodynamic property for estimating the energy involved in the adsorption system [56]. Considering the limitation of the assumption for the Clausius Clapeyron equation that the behaviour of the ideal gas phase and negligible phase volume effect of the adsorbed phase only applies at low pressure and may not be valid at high pressures, Chakraborty et al. [57], proposed a Chakraborty–Saha–Koyama equation (C-S-K) for calculating isosteric heat of adsorption (Q_{st}). The C-S-K was developed based on the principle of equilibrium chemical potential between the adsorbed and the gaseous phase, the equations of state and the Maxwell relations [56]. The Q_{st} was calculated as a function of the sorption potential gradients of pressure and temperature concerning entropy and specific volume. Eq. (7) defines the C-S-K equation to calculate the isosteric heat or adsorption enthalpy Q_{st}. The calculated isosteric heat for the developed composites is furnished in Table 6.

$$Q_{ST=}\ RT^2 \left[\left(\frac{\partial (lnP)}{\partial T}\right)_q\right] + \ T v_g \frac{dP}{dT}(P,T) \tag{7}$$

where, R (J g^{-1} K^{-1}) denotes the gas constant; ν_g (m^3 kg^{-1}) is the specific volume of the adsorbate; q is the Uptake kg/kg; T (K) is the adsorption temperature at corresponding pressure P (kPa).

As shown in Fig. 12, the isosteric heat of adsorption or adsorption enthalpy decreases with increasing uptake. It is because the initial adsorbate molecules adsorb onto the high-energy sorption sites,

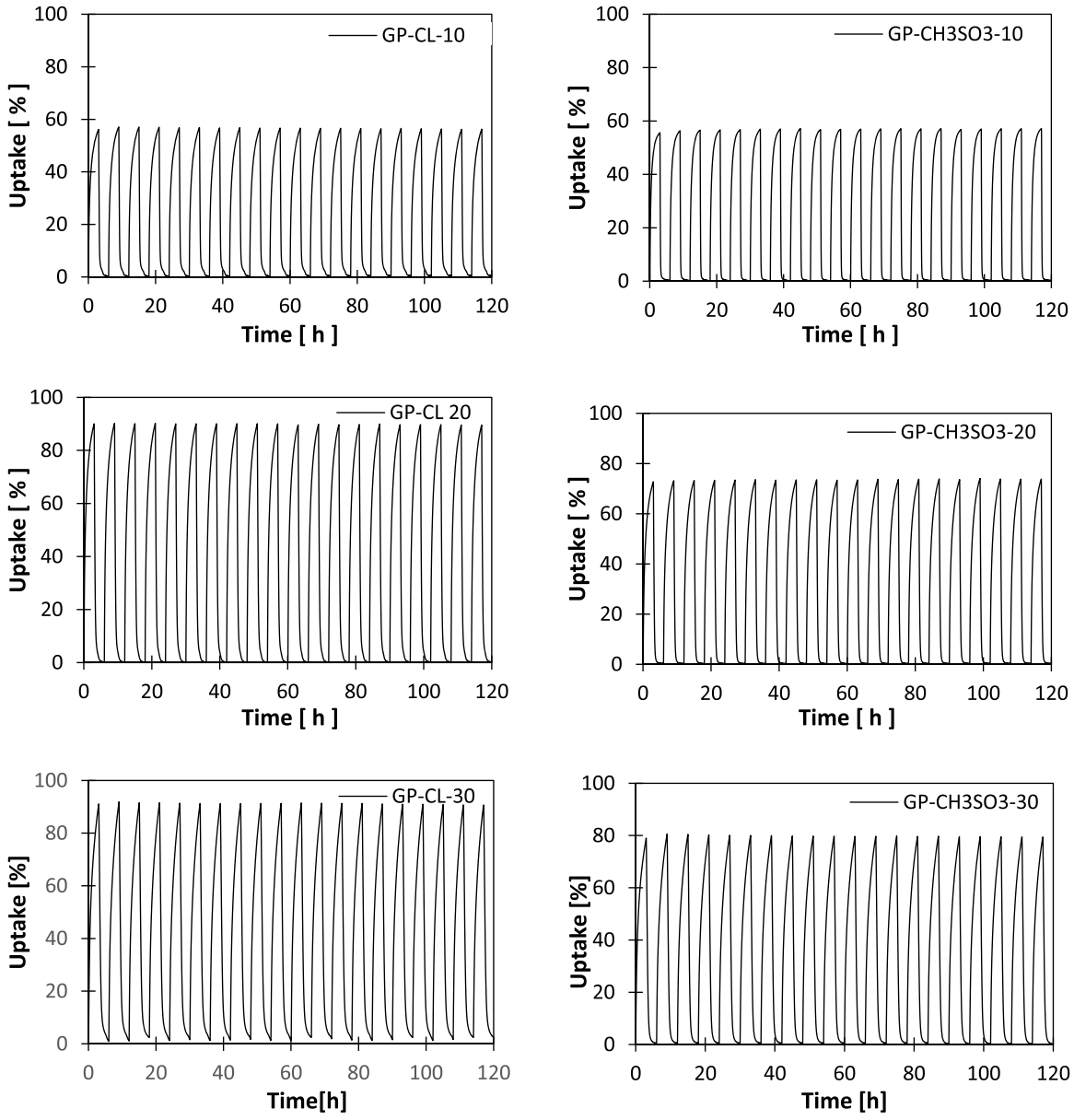

Fig. 10. . Gravimetric water adsorption/desorption cycles for selected composites GP-CL-10, GP-CL-30, GP-CH_3SO_3-10 and GP-CH_3SO_3-30 (stability test).

releasing high amounts of heat energy and resulting in a higher adsorption enthalpy. On the other hand, when the uptake increases, i.e., high-energy sites are saturated with adsorbates, the water molecules get adsorbed onto the sites possessing lower energy, and thus the adsorption enthalpy is seen gradually decreasing.

4. Composites cyclic performance analysis

4.1. Material-level cyclic performance

The material-level cyclic performance based on the adsorption isotherms was performed to understand the cyclic water uptake potential of the developed composites and benchmark them against SG, as shown in Figs. 13 and 14. show the experimental isotherm curves and the cycle operation at the evaporator temperature of 12 °C, condensation temperature 35 °C and desorption 85 °C. The mostly impregnated composites yet stable, i.e., GP-CH_3SO_3-30 and GP-CL-30, were investigated. Investigating the evaporating temperature of <25 °C (P_v = 1.4 kPa) depicts the potential cyclic performance when GP-CH_3SO_3 inferiors that for silica gel and the opposite in case of evaporating temperature ≥25 °C (P_v=3.2).

At the low vapour pressure end of 1.4 kPa corresponding to an evaporator temperature of 12 °C, the net cyclic equilibrium uptake for SG, GP-CH_3SO_3-30 and GP-CL-30 was 0.15 kg/kg, 0.13 kg/kg and 0.18 kg/kg, respectively. SG outperformed GP-CH_3SO_3-30 regarding the net cyclic water uptake shown by distance 1-4, while GP-CL-30 outperforms SG. The two isotherms SG and GP-CH_3SO_3-30 at 35 °C adsorption temperatures intersect at a vapour pressure of 3.2 kPa, which makes GP-CH_3SO_3-30 outperforms SG if the evaporation takes place above 25 °C. As shown in Fig. 14, considering the evaporator, condenser, adsorption and desorption temperatures of 25 °C, 35 °C, 35 °C and 85 °C, the cyclic equilibrium uptake utilising GP-CH_3SO_3-30 and GP-CL-30 outperformed that for SG by 38 % and 54 %, respectively. Practically, a low evaporator temperature requirement might be less concern when utilising desalination, and freshwater production is highly prioritised over cooling, meaning that high evaporator temperature is acceptable. These findings agree with the reported results in the literature by Lian et al. [59] and Banda et al. [60].

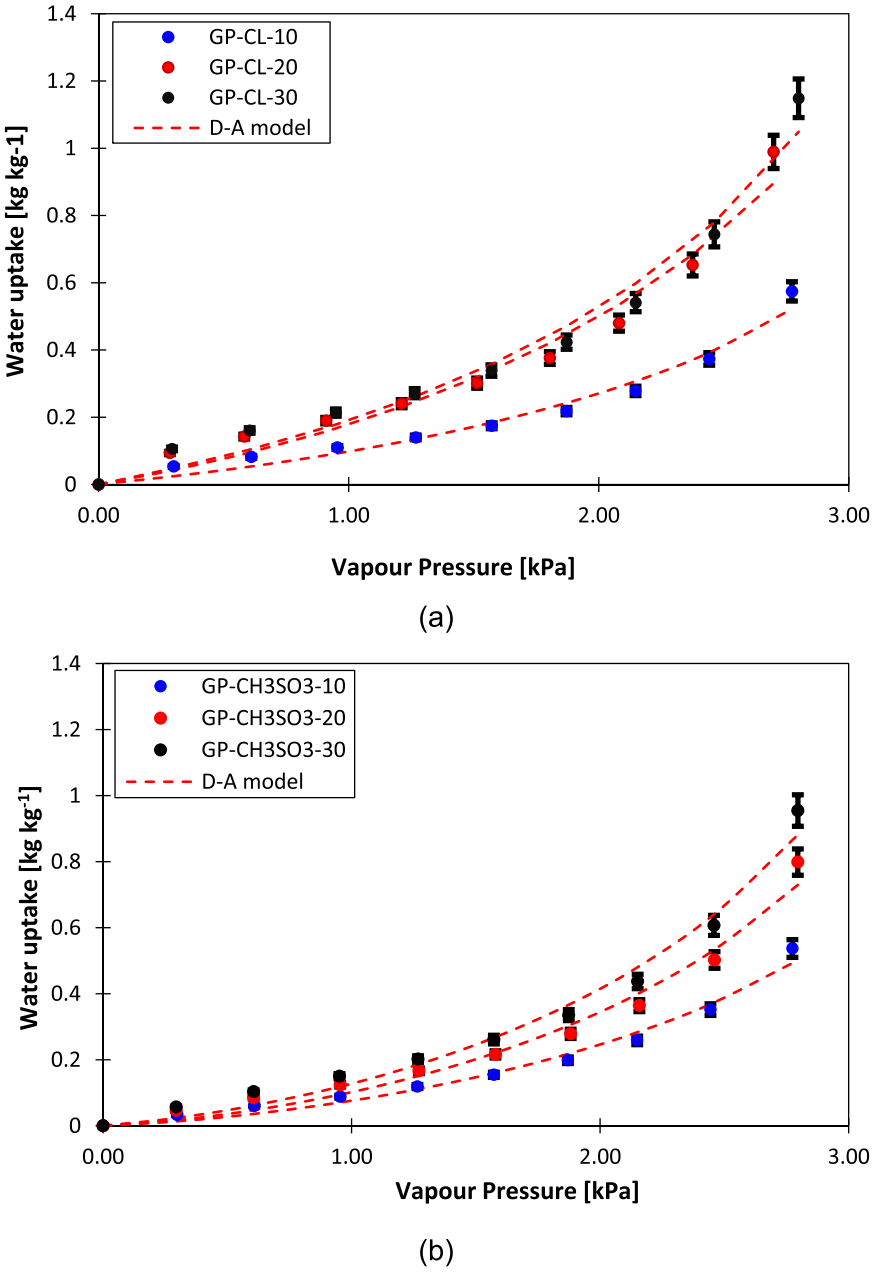

Fig. 11. . Experimental isotherm of composites fitted with the D-A model (a) GP-[EMIM][Cl] and (b) GP- CH_3SO_3.

Table 4
Parameters of the D-A model for the fitted isotherm data for the composites.

Adsorbent	D-A model fitting parameters			RMSD [%]
	Maximum uptake [kgkg^{-1}]	Characteristics energy [kJkg^{-1}]	Heterogeneity parameter [-]	
GP-CL-10	0.89	52.67	0.69	2.57
GP-CL-20	1.50	55.36	0.72	4.65
GP-CL-30	1.70	50.63	0.68	5.01
GP-CH3-SO3-10	0.75	55.18	0.78	2.13
GP-CH3-SO3-20	1.13	50.90	0.77	3.38
GP-CH3-SO3-30	1.41	48.32	0.74	3.68

Table 5
The empirical constants for the LDF.

Parameter	Value		Unit
	GP/IL composite	Silica gel	
D_{so}	4.4E-4	2.54E-4	m^2/s
E_a	48.32–55.36	42	kJ/mol
R_p	2.9 E-4	0.16E-5	m

4.2. *Component-level cyclic performance*

The previous isotherm cyclic analysis considered the material-level equilibrium sorption performance but overlooked the influence of the material's thermal performance, specifically at the component level (i.e., adsorbent bed). Therefore, 2D dynamic heat and mass transfer performance at the adsorbent bed level was undertaken to envisage the influence of the adsorption and thermal characteristics of the developed

Table 6
Isosteric heat of sorption of the developed composites.

Material	Heat of sorption (J/mol)	Material	Heat of sorption (J/mol)
Pure EMIM-CL	31,905	Pure EMIM CH_3SO_3	31,605
GP-CL-10	26,525	GP-CH_3SO_3-10	26,634
GP-CL-20	26,549	GP-CH_3SO_3-20	26,528
GP-CL-30	26,571	GP-CH_3SO_3-30	26,514
Fuji silica gel	26,078	Fuji silica gel [58]	26,790

composites compared to the SG benchmark. The mostly impregnated composites yet stable, i.e., GP-CH_3SO_3-30 and GP-CL-30, were investigated. The cycle time of 800 s, including the 30 s preheating/precooling time, was considered in this analysis. The simulated geometry was a circular finned tube heat exchanger packed with adsorbent materials. Fig. 15 shows the simulated finned tube adsorbent bed, the axisymmetric computational domain and the mesh replicating the simulated geometry. The computational domain considered was half the space between two fins. Banda et al. previously published the details about the simulation model and its validation [60]. Tables 7 and 8 give the geometry dimensions and operating conditions.

Figs. 16 and 17 show cyclic dynamic changes in the adsorbent bed's temperature and water uptake/offtake by utilising evaporator temperatures 12 °C and 25 °C, similar to the evaporator temperatures utilised for analysing the potential cyclic performance based on the adsorption isotherms. Although silica gel outperformed GP-CH_3SO_3-30 based on the isotherm cyclic performance at 12 °C evaporator temperature, its low thermal diffusivity hindered the utilisation of such an adsorption potential as determined by the component level analysis. Therefore, the developed composite, GP-CH3SO3-30 and GP-CL-30, outperformed SG at the component level, utilising evaporator temperatures 12 °C and 25 °C by 75 % and 79 % in terms of water production over the complete cycle. It is primarily due to the relatively faster thermal response of the

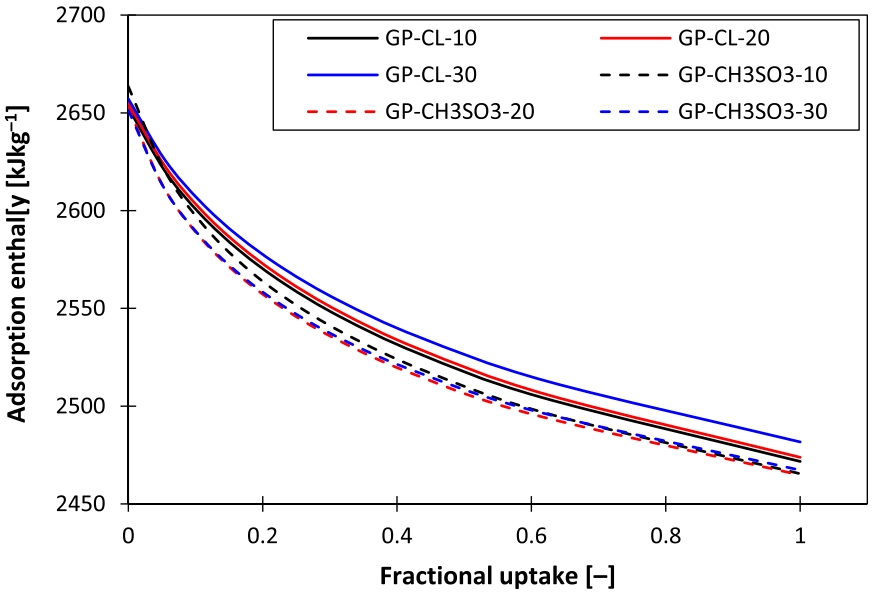

Fig. 12. Isosteric heat of adsorption of the developed composites.

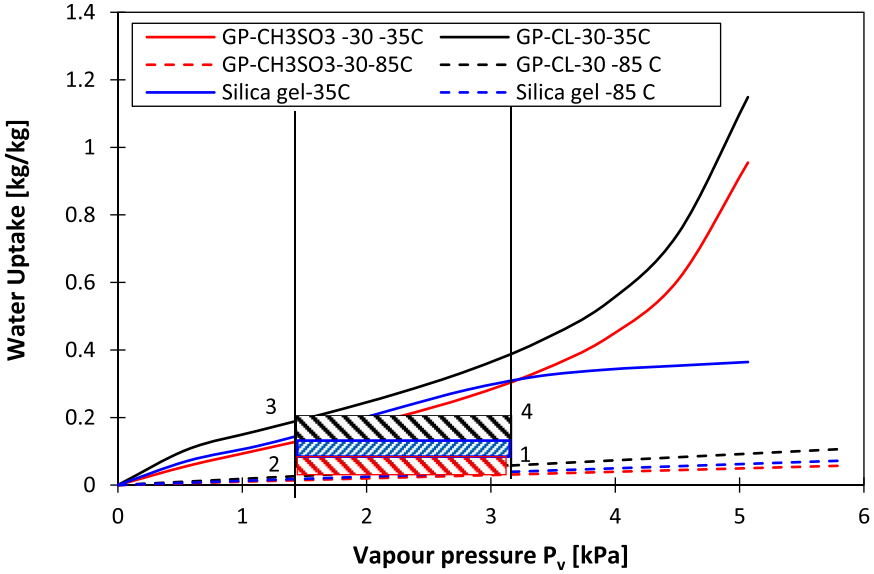

Fig. 13. Comparison of GP-CH_3SO_3-30 and GP-CL-30 and SG at 35 °C, condensation and 85 °C, regeneration temperatures for 12 °C evaporation temperature.

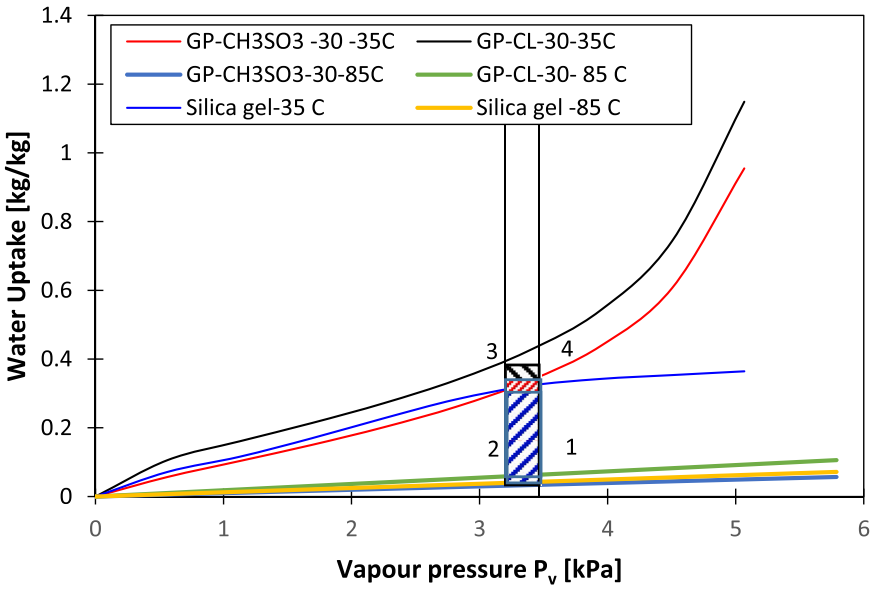

Fig. 14. Comparison of GP-CH_3SO_3-30 and GP-CL-30 and SG at 35 °C, condensation and 85 °C, regeneration temperatures for 25 °C evaporation temperature.

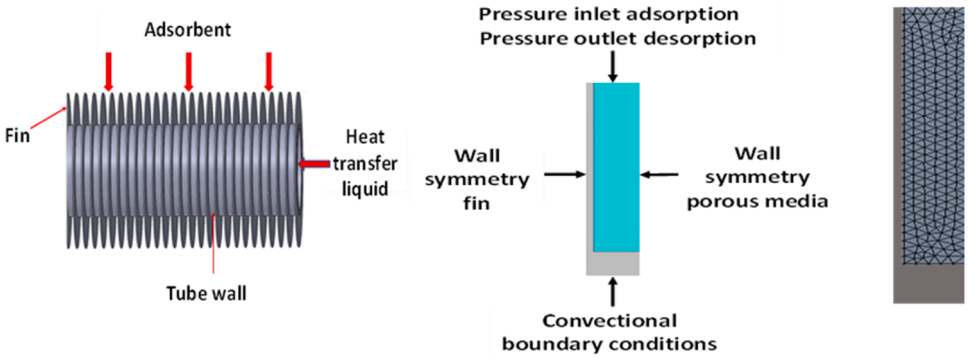

Fig. 15. . Schematic and geometry of the simulated adsorbent bed.

Table 7
Dimensions for the simulation model.

Parameter	Value
Tube outer diameter (d_o)	27 mm
Tube inner diameter (d_i)	24 mm
Fin height (h_f)	10 mm
Fin thickness (δ)	0.54 mm
Fin pitch (p)	3.8 mm
length of the finned tube (l)	500 mm

Table 8
Operating conditions and parameters for the simulation.

Parameter	Value	Unit
$M_{GP/IL}$	0.43	kg
M_{SG}	0.22	kg
M_{hex}	2.02	kg
T_{evap}	12–25	°C
T_{cond}	35	°C
T_{cw}	35	°C
T_{des}	85	°C
T_{ads}	35	°C
T_{chw}	35	°C
$\dot{m}_{ads/des}$	0.036	kg/s
$\dot{m}_{evap}$	0.018	kg/s
$\dot{m}_{cond}$	0.048	kg/s
t_{cycle}	800	s

composites, which is demonstrated by the dynamic temperature profile in Fig. 16 (a–d). At an evaporator temperature of 25 °C, the cumulative advanced adsorption and thermal characteristics of developed composites led to a higher water production by 82 % and 85 % over the entire cycle as shown in Fig. 16 a–d and confirmed in Fig. 17 a–d. Such findings align with previously published research by Banda et al. [60] and Elsheniti et al. [61].

5. Conclusion

This study aimed to develop novel sorption adsorbent composites comprised of GP host matrix and ([EMIM][CH_3SO_3] and [EMIM][Cl], individually) ILs as adsorbents, as well as determine the material and component levels cyclic performances. Initially, eight composites were developed utilising few-layered graphene as a host matrix and ILs at different concentrations, which, according to practical application concerns of hydrated ILs agglomeration due to IL over-impregnation, the study focused on six composites, namely GP-CL-10, 20 & 30 and GP-CH_3SO_3-10, 20 & 30. The adsorption and thermal properties of the composites were experimentally determined and benchmarked against the baseline silica gel adsorbent, while the component level performance was investigated *via* 2D heat and mass transfer dynamic modelling using a previously validated model. The key findings of the study are concluded below.

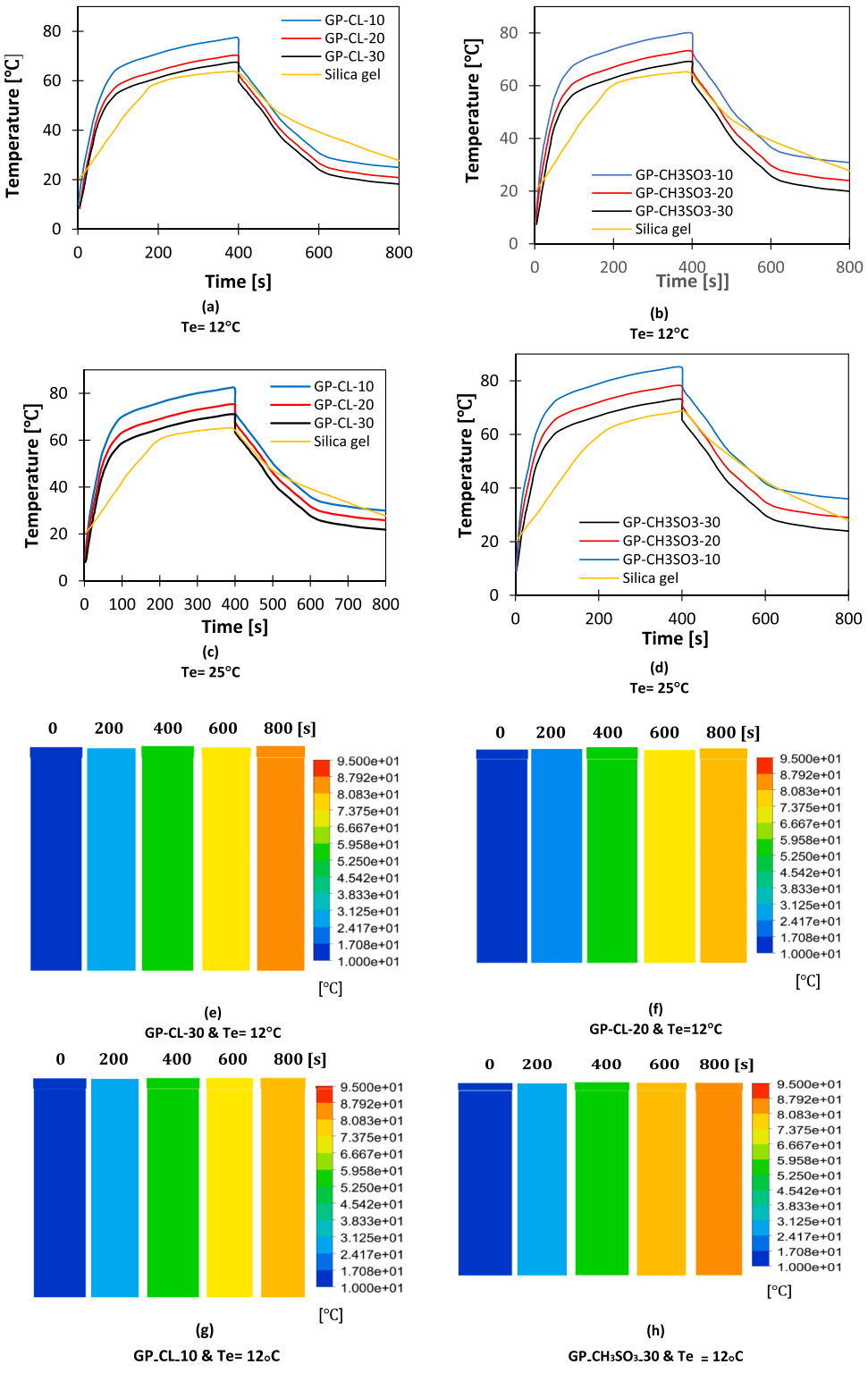

Fig. 16. Dynamic temperature profiles for GP-Cl-10-30 and GP-CH_3SO_3-10-30.

- ILs have a considerable influence on the water uptake of the composites. Complete impregnation occurred with a high thermophysical stability level in composites of 65 % IL content and below. The equilibrium adsorption water uptake increased with increasing the IL content, as shown in the GP-CL-30, which was 78 % more than the baseline Silica gel. The results also showed that the high concentration [EMIM][CL] is more effective than [EMIM][CH_3SO_3] counterpart in terms of water solvation compared to the and had the effect of increasing water uptake.
- GP's high thermal diffusivity enhanced the developed composites' thermal response. The composites at low IL content showed superior thermal diffusivity with the highest value of 11.84 mm^2/s for the GP-CH3SO3-10, 394 times higher than Silica gel.

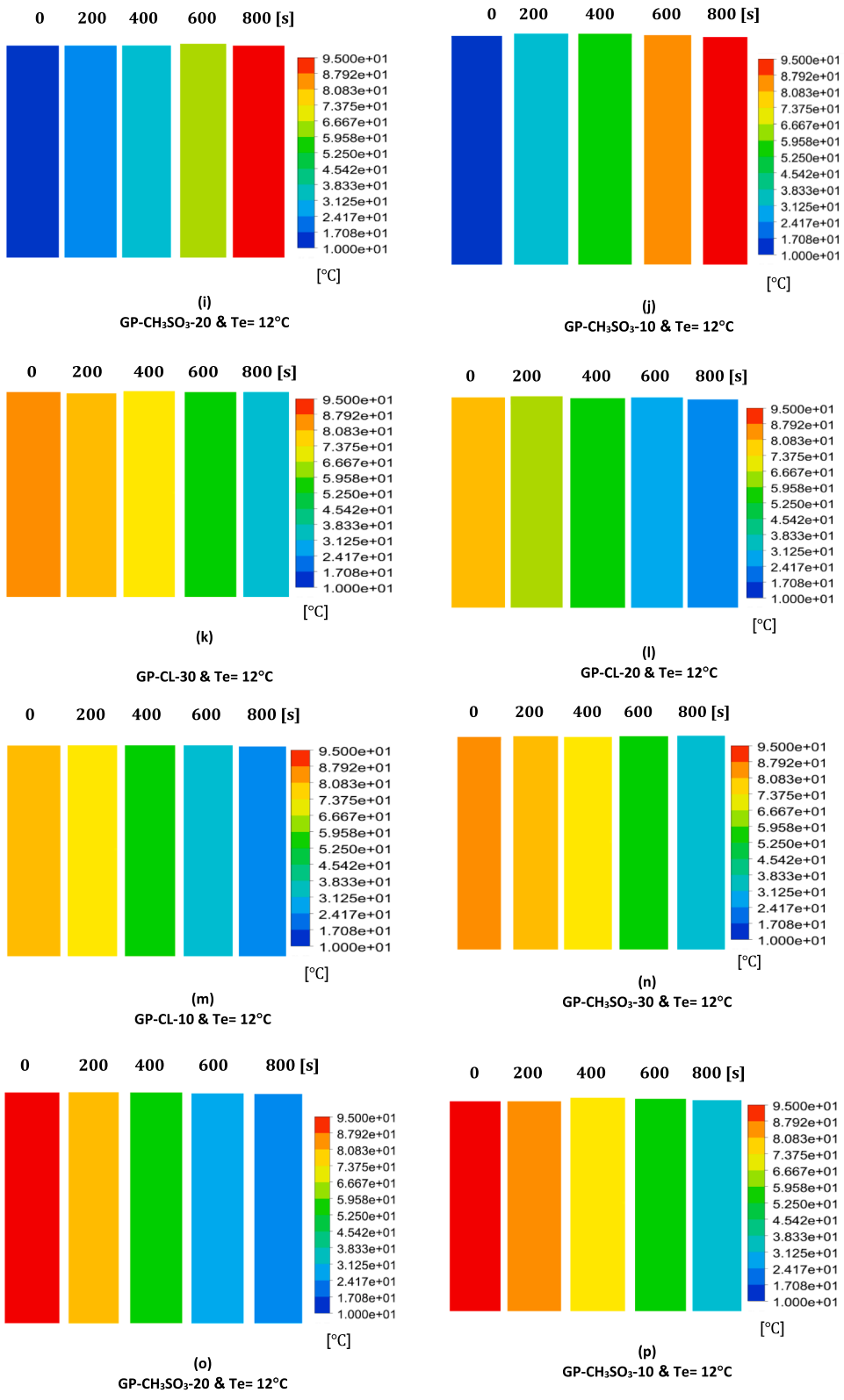

Fig. 16. (*continued*).

- GP-CL-30 can be considered the most suitable among the investigated materials for cooling and water desalination productivity among the developed composites. However, its positive influence is even more distinctive when prioritising desalination over cooling.

CRediT authorship contribution statement

Handsome Banda: Investigation, Resources, Data curation. **Tahmid Hasan Rupam:** Investigation, Resources, Data curation. **Ahmed Rezk:** Conceptualization, Methodology. **Zoran Visak:** Writing – review & editing, Formal analysis. **James Hammerton:** Investigation, Resources,

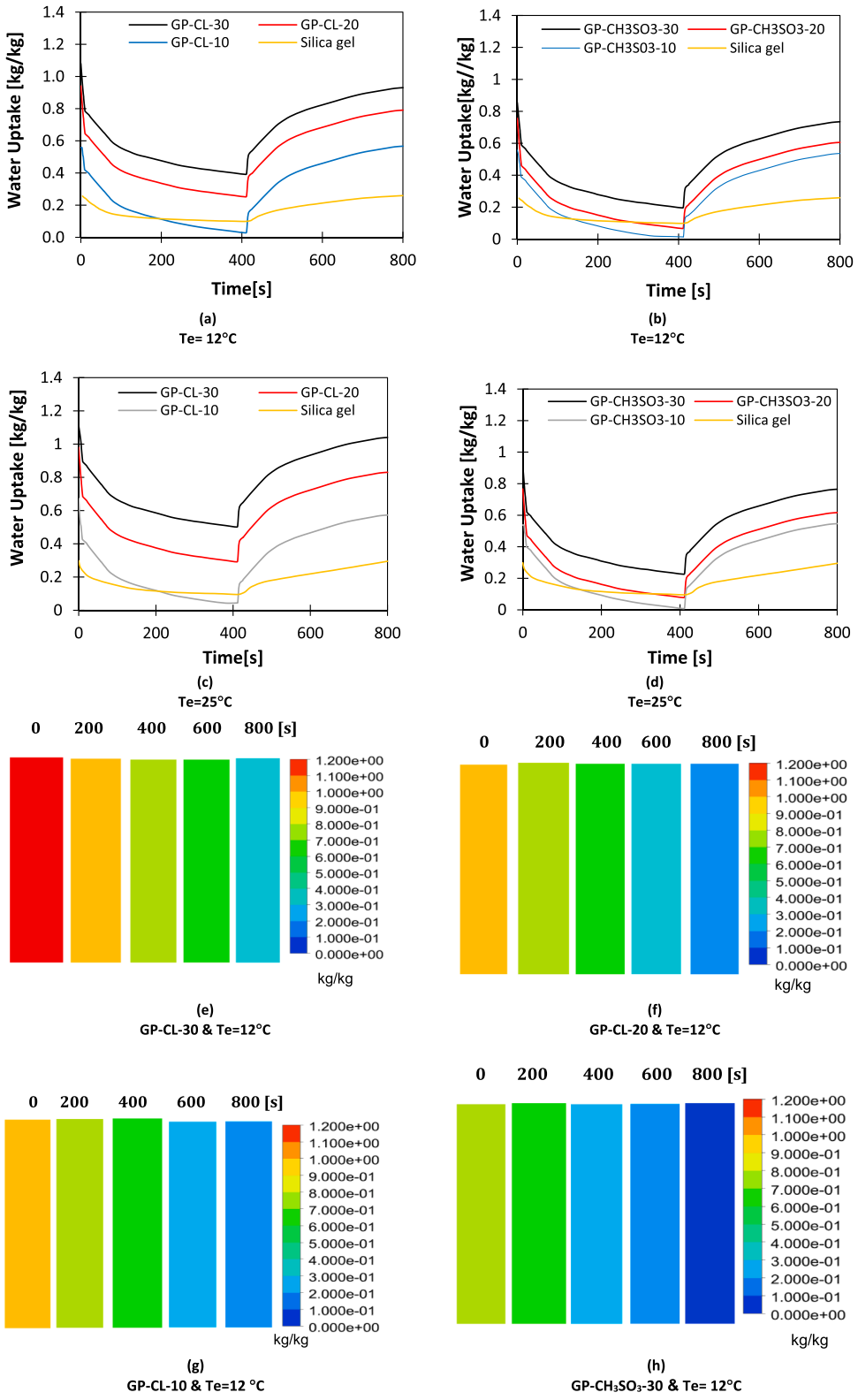

Fig. 17. Dynamic uptake profiles for GP-Cl-10-30 and GP-CH_3SO_3-10-30.

Data curation. **Qingchun Yuan:** Investigation, Resources, Data curation. **Bidyut Baran Saha:** Writing – review & editing, Formal analysis.

Declaration of Competing Interest

The authors declare the following financial interests/personal relationships which may be considered as potential competing interests:

Equipment, drugs, or supplies was provided by The Royal Society.

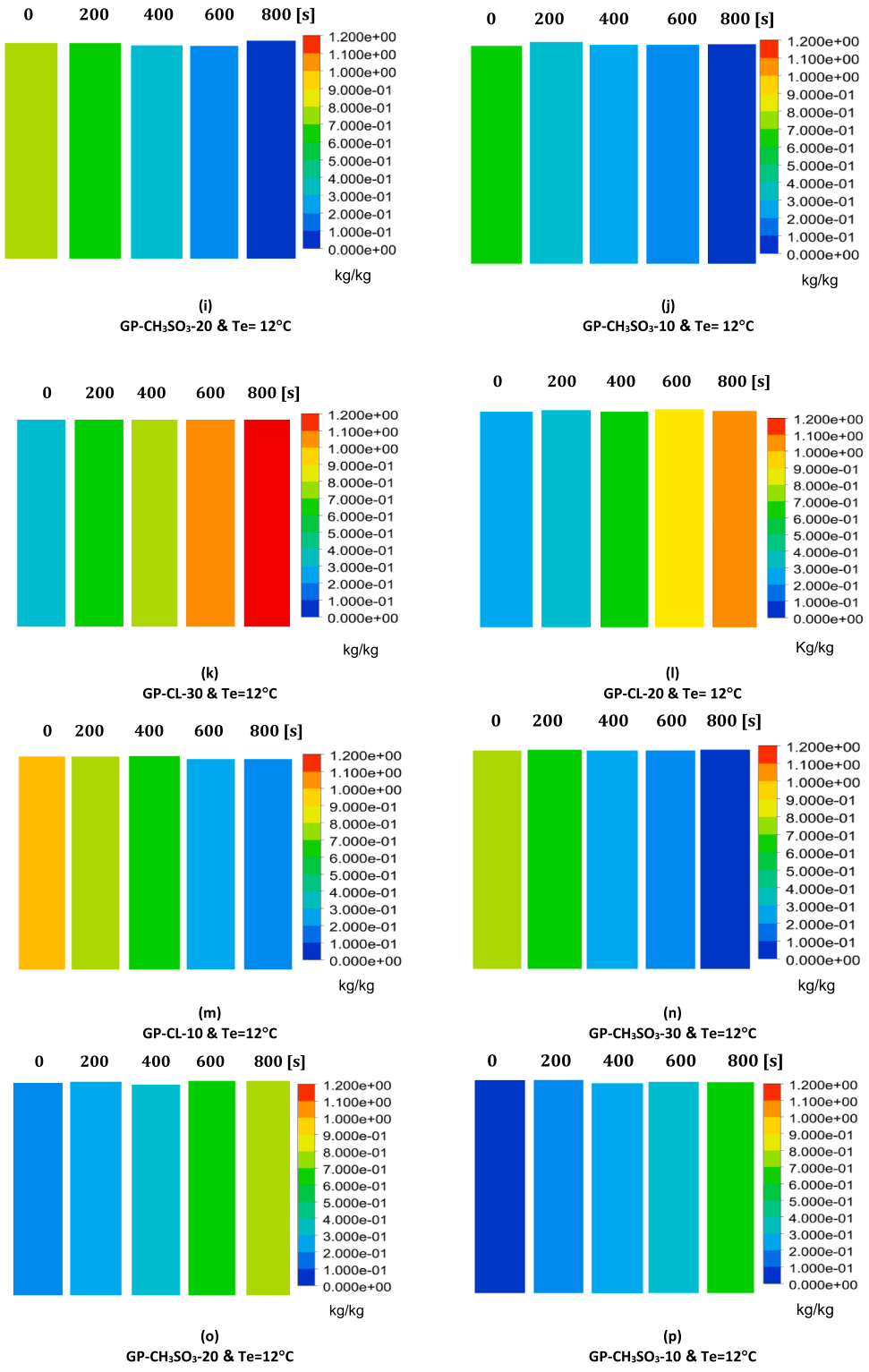

Fig. 17. (*continued*).

Ahmed Rezk has patent pending to GB2207186.4. Zoran Visak has patent pending to GB2207186.4. No other activities or relationships that cause a conflict of interest

Data availability

Data will be made available on request.

Acknowledgment

This work was supported by The Royal Society (grant no. IES\R3 \203128).

References

[1] A.S. Alsaman, et al., A state of the art of hybrid adsorption desalination–cooling systems, Desalination 58 (2016) 692–703.

[2] C.Y. Tso, et al., Experimental performance analysis on an adsorption cooling system using zeolite 13X/CaCl2 adsorbent with various operation sequences, Int. J. Heat Mass Transf. 85 (2015) 343–355.
[3] H.M. Asfahan, et al., Evaluating the emerging adsorbents for performance improvement of adsorption desalination cum cooling system, Int. Commun. Heat Mass Transf. 142 (2023), 106661.
[4] S. Jribi, et al., CFD simulation and experimental validation of ethanol adsorption onto activated carbon packed heat exchanger, Int. J. Refrig. 74 (2017) 345–353.
[5] M. Sharifzadeh, M. Ghazikhani, H. Niazmand, Temporal exergy analysis of adsorption cooling system by developing non-flow exergy function, Appl. Therm. Eng. 139 (2018) 409–418.
[6] M. Khanam, et al., Numerical investigation of small-scale adsorption cooling system performance employing activated carbon-ethanol pair, Energies 11 (6) (2018) 1499.
[7] Y.-D. Kim, K. Thu, K.C. Ng, Adsorption characteristics of water vapor on ferroaluminophosphate for desalination cycle, Desalination 344 (2014) 350–356.
[8] S.-Y. Woo, et al., Silica gel-based adsorption cooling cum desalination system: Focus on brine salinity, operating pressure, and its effect on performance, Desalination 467 (2019) 136–146.
[9] T. Bujok, et al., Analysis of designs of heat exchangers used in adsorption chillers, Energies 14 (2021), https://doi.org/10.3390/en14238038.
[10] K. Grabowska, et al., Experimental Investigation of an Intensified Heat Transfer Adsorption Bed (IHTAB) Reactor Prototype, Materials 14 (2021), https://doi.org/10.3390/ma14133520.
[11] D. Skrobek, et al., Prediction of sorption processes using the deep learning methods (long short-term memory), Energies 13 (2020), https://doi.org/10.3390/en13246601.
[12] J. Krzywanski, et al., Heat and mass transfer prediction in fluidized beds of cooling and desalination systems by AI approach, Appl. Therm. Eng. 225 (2023), 120200.
[13] K. Thu, et al., Performance investigation of a waste heat-driven 3-bed 2-evaporator adsorption cycle for cooling and desalination, Int. J. Heat Mass Transf. 101 (2016) 1111–1122.
[14] B. Han, A. Chakraborty, Experimental investigation for water adsorption characteristics on functionalized MIL-125 (Ti) MOFs: Enhanced water transfer and kinetics for heat transformation systems, Int. J. Heat Mass Transf. 186 (2022), 122473.
[15] Y.Y. Tanashev, A.V. Krainov, Y.I. Aristov, Thermal conductivity of composite sorbents “salt in porous matrix” for heat storage and transformation, Appl. Therm. Eng. 61 (2) (2013) 401–407.
[16] K.C. Chan, et al., Performance predictions for a new zeolite 13X/CaCl2 composite adsorbent for adsorption cooling systems, Int. J. Heat Mass Transf. 55 (11) (2012) 3214–3224.
[17] C.Y. Tso, C.Y.H. Chao, Activated carbon, silica-gel and calcium chloride composite adsorbents for energy efficient solar adsorption cooling and dehumidification systems, Int. J. Refrig. 35 (6) (2012) 1626–1638.
[18] Y.I. Aristov, et al., Reallocation of adsorption and desorption times for optimisation of cooling cycles, Int. J. Refrig. 35 (3) (2012) 525–531.
[19] A. Kulakowska, et al., Effect of metal and carbon nanotube additives on the thermal diffusivity of a silica gel-based adsorption bed, Energies 13 (2020), https://doi.org/10.3390/en13061391.
[20] T. Maruyama, S. Thomas, et al., Chapter 6 - carbon nanotubes. Handbook of Carbon-Based Nanomaterials, Elsevier, 2021, pp. 299–319. Editors.
[21] I. Tlili, et al., Investigation of thermal characteristics of carbon nanotubes: measurement and dependence, J. Mol. Liq. 294 (2019), 111564.
[22] I.A. Kinloch, et al., Composites with carbon nanotubes and graphene: an outlook, Science 362 (6414) (2018) 547–553.
[23] A. Pal, et al., Activated carbon and graphene nanoplatelets based novel composite for performance enhancement of adsorption cooling cycle, Energy Convers. Manag. 180 (2019) 134–148.
[24] F. Li, L. Long, Y. Weng, A Review on the contemporary development of composite materials comprising graphene/graphene derivatives, Adv. Mater. Sci. Eng. 2020 (2020), 7915641.
[25] J. Sturala, et al., Chemistry of graphene derivatives: synthesis, applications, and perspectives, Chemistry 24 (23) (2018) 5992–6006.
[26] M. Shtein, et al., Characterization of graphene-nanoplatelets structure *via* thermogravimetry, Anal. Chem. 87 (8) (2015) 4076–4080.
[27] S. Ren, P. Rong, Q. Yu, Preparations, properties and applications of graphene in functional devices: a concise review, Ceram. Int. 44 (11) (2018) 11940–11955.
[28] X.J. Lee, et al., Review on graphene and its derivatives: Synthesis methods and potential industrial implementation, J. Taiwan Inst. Chem. Eng. 98 (2019) 163–180.
[29] H.V. Madhad, et al., Graphene/graphene nanoplatelets reinforced polyamide nanocomposites: a review, High Perform. Polym. 33 (9) (2021) 981–997.
[30] Y. Geng, S.J. Wang, J.-K. Kim, Preparation of graphite nanoplatelets and graphene sheets, Colloid Interface Sci. 336 (2) (2009) 592–598.
[31] A. Jiménez-Suárez, S. Prolongo, Graphene nanoplatelets, MDPI Appl. Sci. 10 (2020) 1753.
[32] I.I. El-Sharkawy, et al., A study on consolidated composite adsorbents for cooling application, Appl. Therm. Eng. 98 (2016) 1214–1220.
[33] A.C. Gautam, S. Sahoo, Experimental investigation on adsorbent composites for CO_2 capture application: an attempt to improve the dynamic performance of the parent adsorbent, Int. J. Heat Mass Transf. 203 (2023), 123796.
[34] M.D. Joshi, J.L. Anderson, Recent advances of ionic liquids in separation science and mass spectrometry, RSC Adv. 2 (13) (2012) 5470–5484.
[35] A.A. Hassan, et al., Development of novel ionic liquid-based silica gel composite adsorbents for designing high-efficiency adsorption heat pumps, Int. Commun. Heat Mass Transf. 146 (2023), 106862.
[36] J. Yuan, et al., Amine-functionalized poly(ionic liquid) brushes for carbon dioxide adsorption, Chem. Eng. J. 316 (2017) 903–910.
[37] A.A. Askalany, A. Freni, G. Santori, Supported ionic liquid water sorbent for high throughput desalination and drying, Desalination 452 (2019) 258–264.
[38] A.A. Askalany, et al., Water desalination by silica supported ionic liquid: adsorption kinetics and system modeling, Energy 239 (2022), 122069.
[39] A. Pal, et al., Ionic liquid as a new binder for activated carbon based consolidated composite adsorbents, Chem. Eng. J. 326 (2017) 980–986.
[40] K.C. Ng, et al., Experimental investigation of the silica gel–water adsorption isotherm characteristics, Appl. Therm. Eng. 21 (16) (2001) 1631–1642.
[41] K. Thu, et al., Thermo-physical properties of silica gel for adsorption desalination cycle, Appl. Therm. Eng. 50 (2) (2013) 1596–1602.
[42] Y. Zhao, et al., Measurements of ionic liquids thermal conductivity and thermal diffusivity, J. Therm. Anal. Calorim. 128 (1) (2017) 279–288.
[43] H.T. Chua, et al., Adsorption characteristics of silica gel + water systems, J. Chem. Eng. Data 47 (5) (2002) 1177–1181.
[44] R. Syah, et al., Artificial intelligence simulation of water treatment using nanostructure composite ordered materials, J. Mol. Liq. 345 (2022), 117046.
[45] A.B. Albadarin, et al., Activated lignin-chitosan extruded blends for efficient adsorption of methylene blue, Chem. Eng. J. 307 (2017) 264–272.
[46] A. Ghasemi, et al., Using quantum chemical modeling and calculations for evaluation of cellulose potential for estrogen micropollutants removal from water effluents, Chemosphere, 178 (2017) 411–423.
[47] S.K. Bhagat, T.M. Tung, Z.M. Yaseen, Development of artificial intelligence for modeling wastewater heavy metal removal: State of the art, application assessment and possible future research, J. Clean. Prod. 250 (2020), 119473.
[48] K.Y. Foo, B.H. Hameed, Insights into the modeling of adsorption isotherm systems, Chem. Eng. J. 156 (1) (2010) 2–10.
[49] A. Malek, S. Farooq, Comparison of isotherm models for hydrocarbon adsorption on activated carbon, AIChE J. 42 (11) (1996) 3191–3201.
[50] M. Muttakin, et al., Theoretical framework to evaluate minimum desorption temperature for IUPAC classified adsorption isotherms, Int. J. Heat Mass Transf. 122 (2018) 795–805.
[51] A. Gil, P. Grange, Application of the Dubinin–Radushkevich and Dubinin–Astakhov equations in the characterization of microporous solids, Colloids Surf. A Physicochem. Eng. Asp. 113 (1) (1996) 39–50.
[52] T.H. Rupam, et al., Thermodynamic property surfaces for various adsorbent/adsorbate pairs for cooling applications, Int. J. Heat Mass Transf. 144 (2019), 118579.
[53] A. Chakraborty, et al., On the Thermodynamic Modeling of the Isosteric Heat of Adsorption and Comparison with Experiments, Appl. Phys. Lett. 89 (2006), 171901.
[54] Y. Zhang, V. Palomba, A. Frazzica, Understanding the effect of materials, design criteria and operational parameters on the adsorption desalination performance – a review, Energy Convers. Manag. 269 (2022), 116072.
[55] I.I. El-Sharkawy, et al., Adsorption of ethanol onto parent and surface treated activated carbon powders, Int. J. Heat Mass Transf. 73 (2014) 445–455.
[56] I. Jahan, et al., Energy efficient green synthesized MOF-801 for adsorption cooling applications, J. Mol. Liq. 345 (2022), 117760.
[57] A. Chakraborty, et al., On the thermodynamic modeling of the isosteric heat of adsorption and comparison with experiments, Appl. Phys. Lett. 89 (17) (2006), 171901.
[58] S. Mitra, et al., Modeling study of two-stage, multi-bed air cooled silica gel+water adsorption cooling cum desalination system, Appl. Therm. Eng. 114 (2017) 704–712.
[59] B. Lian, et al., Extraordinary water adsorption characteristics of graphene oxide, Chem. Sci. 9 (22) (2018) 5106–5111.
[60] H. Banda, et al., Experimental and computational study on utilising graphene oxide for adsorption cooling and water desalination, Appl. Therm. Eng. 229 (2023), 120631.
[61] M.B. Elsheniti, et al., Performance of a solar adsorption cooling and desalination system using aluminum fumarate and silica gel, Appl. Therm. Eng. 194 (2021), 117116.